Available online at www.sciencedirect.com

ScienceDirect

Ceramics International 40 (2014) 429–435

CERAMICS INTERNATIONAL

www.elsevier.com/locate/ceramint

One-pot triethanolamine-assisted hydrothermal synthesis of Ag/ZnO heterostructure microspheres with enhanced photocatalytic activity

Bo Chai*, Xing Wang, Siqing Cheng, Huan Zhou, Fen Zhang

School of Chemical and Environmental Engineering, Wuhan Polytechnic University, Wuhan 430023, PR China

Received 7 May 2013; received in revised form 10 June 2013; accepted 10 June 2013
Available online 18 June 2013

Abstract

The Ag/ZnO heterostructure microspheres were prepared *via* a simple one-pot triethanolamine (TEA)-assisted hydrothermal route and characterized by X-ray diffraction (XRD), Field Emission Scanning Electron Microscopy (FESEM), X-ray Photoelectron Spectroscopy (XPS), UV–vis Diffuse Reflectance Absorption Spectra (DRS) and Photoluminescence Spectra (PL), demonstrating that Ag nanoparticles were attached on the surface of ZnO microspheres. The photocatalytic degradation of Rhodamine B (RhB) by the as-synthesized Ag/ZnO microspheres was investigated and optimized, indicating the best photocatalytic performance of Ag/ZnO of 1:150 (mol/mol). This may be attributed to the charge separation of photogenerated electrons and holes by Ag/ZnO heterostructure microspheres, which is interpreted by the proposed mechanism for Ag/ZnO heterostructure microspheres as catalyst.

Keywords: Ag/ZnO heterostructure microsphere; Hydrothermal synthesis; Photocatalytic activity; Triethanolamine

1. Introduction

Semiconductor photocatalytic process is a promising advanced oxidation technology for environmental remediation. Among these semiconductor photocatalysts, TiO_2 has been extensively and deeply investigated because of its high photosensitivity and nontoxicity [1,2]. ZnO as a direct wide band-gap (3.37 eV) semiconductor has been considered as a suitable alternative to TiO_2 due to its similar band-gap energy with TiO_2 and lower cost [3]. Moreover, larger quantum efficiency and higher photocatalytic activity than TiO_2 have been reported [4,5]. However, the photocatalytic activity of ZnO should be further enhanced from the viewpoint of practical use. Therefore, various methods have been developed to reduce the charge recombination of ZnO, and then improve its photocatalytic activity [6–8].

Ag as an electron sink is proposed to allow electrons transfer from ZnO to Ag through the interface when coupled with ZnO, which benefits the separation of photogenerated electron–hole pairs, and enhancing the photocatalytic activity. In recent years, the Ag/ZnO heterostructure composites with different morphologies have been successfully synthesized by different methods. Wang et al. prepared the 3D Ag/ZnO hollow microspheres with different Ag contents through a facile one-pot hydrothermal method assisted by sodium alginate [9]. Fu's groups fabricated the Ag/ZnO microspheres by one-pot strategy in ethylene glycol medium [10]. Meng et al. synthesized the 3D fluffy structure Ag/ZnO microspheres *via* one-pot solvothermal route in the presence of citric acid, NaOH and ethanol [11]. Zheng's groups prepared the Ag/ZnO nanocrystals through a simple solvothermal method in the presence of NaOH/ethanol solution [12]. Pan et al. fabricated the Ag/ZnO nanofibers by electrospinning method [13]. Gao et al. prepared the Ag/ZnO nanocomposites with hierarchical micro/nanostructure by the hydrothermal route in the presence of bovine serum albumin [14]. Dendrite-like ZnO@Ag

*Corresponding author. Tel./fax.: +86 27 8394 3956.
E-mail address: willycb@163.com (B. Chai).

0272-8842/$ - see front matter © 2013 Elsevier Ltd and Techna Group S.r.l. All rights reserved.
http://dx.doi.org/10.1016/j.ceramint.2013.06.019

heterostructure nanocrystals were designed and fabricated by a facial two-step chemical method in a large scale [15]. Mudring reported the facile preparation of Ag/ZnO nanoparticles *via* the photoreduction method [16]. Although there are some reports on Ag/ZnO nanocomposites, the developing a facile route to forming Ag/ZnO heterostructure would be still a challenge.

Recently, several groups synthesized ZnO nanostructures by the addition of triethanolamine (TEA) aqueous solution *via* hydrothermal route [17–19]. Meanwhile, the TEA as reducing reagent is well demonstrated in the synthesis of Cu/Cu_2O microcrystal through hydrothermal process [20]. In this case, the multifunctional properties of TEA could simplify the synthesis of Ag/ZnO composite. Herein, we report the successful fabrication of Ag/ZnO heterostructure microspheres *via* a simple TEA-assisted hydrothermal route. Experimental results indicated that Ag/ZnO heterostructure microspheres could be obtained through a one-pot reaction. The photocatalytic activity of the as-prepared Ag/ZnO samples with different Ag contents for degradation of Rhodamine B (RhB) was explored.

2. Experimental

2.1. Material preparation

All chemicals are analytical grade and used as received without further purification. According to the previous report, the volume ratio of TEA to H_2O has an important effect on the morphology of obtained ZnO [17]. Thus, the volume ratio of TEA to H_2O was determined to 1:4 in the all experiment processes. In a typical procedure, 5 mmol $Zn(NO_3)_2 \cdot 6H_2O$ was dissolved in 60 mL of distilled water, then 0.333 mL of $AgNO_3$ solution (0.1 M) and 15 mL of TEA were added under constant stirring at room temperature to ensure well dispersion of the reactant. After stirring for 30 min, the mixed solution was transferred into a 100 mL Teflon-lined stainless steel autoclave and kept at 180 °C for 12 h. The obtained products were collected using centrifugation and washed with water and ethanol for several times, then dried at 80 °C overnight. In this case, the sample was denoted as 1:150 Ag/ZnO (1:150 was the molar ratio of Ag to ZnO based on initial amount of $AgNO_3$ and $Zn(NO_3)_2 \cdot 6H_2O$). The 1:50 Ag/ZnO, 1:100 Ag/ZnO and 1:200 Ag/ZnO composites were also prepared by tuning the initial molar ratio of $AgNO_3$ to $Zn(NO_3)_2 \cdot 6H_2O$. For comparison, the single ZnO was synthesized following the same procedure as above except adding $AgNO_3$.

2.2. Material characterization

The products were characterized by XRD patterns using Bruker D8 Advance X-ray diffractometer with Cu-Kα irradiation ($\lambda = 0.154178$ nm) at 40 kV and 40 mA. The morphology of sample was investigated by JSM-6700F FESEM. XPS measurement was performed on a Kratos XSAM 800 with Mg-Kα source operation at 200 W. DRS was obtained by a Shimadzu UV-3600 spectrophotometer equipped with an integrating sphere using $BaSO_4$ as the reference sample. PL was measured at room temperature on the F-4500 fluorescence spectrophotometer with excitation wavelength at 315 nm.

2.3. Photocatalytic activity test

The photocatalytic activity was evaluated by using RhB as a representative dye pollutant. The detailed procedure was as follows: 0.1 g catalysts and 50 mL of 1×10^{-5} mol/L RhB aqueous solution were mixed in a 50 mL beaker. After stirring under dark for 30 min to reach the adsorption equilibrium, the mixture was irradiated with 19 W UV-light (254 nm) for a given time under continuously stirring. After UV light irradiation for every 10 min, the reaction solution was taken out to measure the concentration change of RhB. The TU-1810 spectrometer was used to measure the concentration of RhB solution before and after photocatalytic reaction by means of the optical characteristic absorption of RhB at ca. 554 nm.

2.4. Detection of hydroxyl radicals (•OH)

The formation of hydroxyl radicals (•OH) at the illuminated photocatalyst/water interface can be detected by PL technique using terephthalic acid (TA) as a probe molecule. Experimental procedures were similar to the measurement of the photocatalytic activity except that the RhB aqueous solution was replaced by the 5×10^{-4} M TA aqueous solution with a concentration of 2×10^{-3} M NaOH solution. PL spectra of the generated 2-hydroxyterephthalic acid were measured on a Varian Cary Eclipase fluorescence spectrophotometer. After light irradiation every 10 min, the reaction solution was used to measure the increase of PL intensity at 425 nm [21,22].

3. Results and discussion

3.1. XRD analysis

Fig. 1 shows the XRD patterns of pure ZnO and Ag/ZnO samples with different Ag contents. All the diffraction peaks could be categorized into two sets. Peaks marked with "#" match well with the standard wurtzite structure ZnO (JCPDS, No. 36-1451), while others marked with "*" agree well with

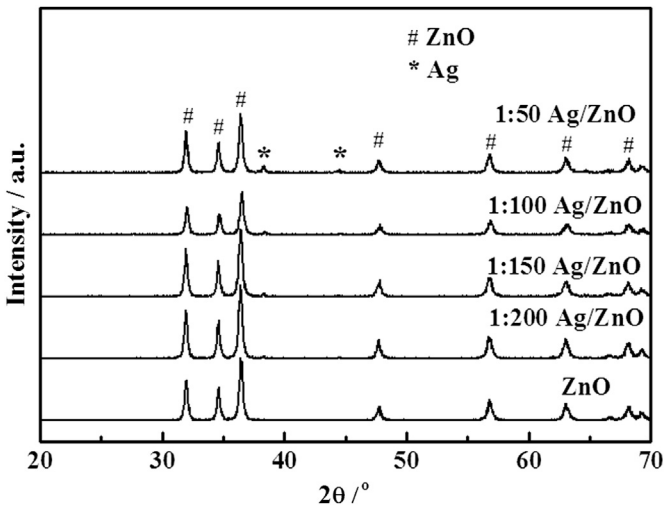

Fig. 1. XRD patterns of pure ZnO and Ag/ZnO composites with different Ag contents.

face-centered cubic silver metal (JCPDS, No. 04-0783) [9]. With increasing silver contents, the corresponding diffraction peak intensity enhanced. No any other crystal phase diffraction peak was detected, indicating the purity of the samples. In addition, negligible changes of all diffraction peak positions and lattice parameters of ZnO in the all Ag/ZnO samples suggested that silver ions were not incorporated into the ZnO lattice, but as metal deposited on the surface.

3.2. SEM characterization and possible formation mechanism of Ag/ZnO composite

The representative SEM images of pure ZnO and Ag/ZnO with molar ratio of 1:150 are shown in Fig. 2a–d. As seen in Fig. 2a, the ZnO microspheres had been successfully prepared by using the TEA aqueous solution under hydrothermal conditions. The magnified SEM image (Fig. 2b) clearly showed that the ZnO microspheres were composed of small nanoparticles with diameters of tens of nanometer, which agreed with the previous report [17]. As shown in Fig. 2c, the Ag/ZnO composite also presented microspherical structure, indicating that adding $AgNO_3$ had not influence on the ZnO aggregation into microspheres. However, the diameters of Ag/ZnO microspheres were bigger than single ZnO. Fig. 2d exhibited the SEM image with higher magnification of the Ag/ZnO composite, showing clearly silver nanoparticles with the diameter of 200–300 nm on the surface of ZnO microspheres.

Based on the above observations, a possible formation mechanism is proposed. In our experiments, the TEA plays a dual role in the formation process of Ag/ZnO microspheres. When the TEA is added into the reaction system under constant stirring, and then the pH value of mixture solution increases, the $[Zn(OH)_4]^{2-}$ is obtained by the reaction of Zn^{2+} and OH^-. And then, the TEA could coordinate with $[Zn(OH)_4]^{2-}$ and form a stable complex of $[Zn(OH)_4]^{2-}$-TEA. At elevated hydrothermal temperature, these complexes break up to release H_2O, ZnO particles would be formed and the TEA molecules are adsorbed on the surface of ZnO. Driven by the minimization of the total energy of the system, ZnO particles could be self-assembled into hierarchical microspheres, which could be called aggregation-based mechanism. Meanwhile, the TEA acts as the reducing agent facilitating Ag^+ transformation into Ag nanoparticles in the chemical reaction process under the hydrothermal conditions.

3.3. XPS analysis

The XPS measurement was carried out to further determine the chemical composition and valence state of various species. Fig. 3a displays the XPS survey spectrum for 1:150 Ag/ZnO composite. As expected, it contained Zn, O and Ag elements. The high-resolution Zn2p spectrum is shown in Fig. 3b, the peaks with binding energy of 1044.3 and 1021.2 eV could be attributed to $Zn2p_{1/2}$ and $Zn2p_{3/2}$, which confirms that Zn element exists mainly in the form of Zn^{2+}. From Fig. 3c, it could be seen that two peaks centered at 367.4 eV and 373.4 eV are assigned to $Ag3d_{5/2}$ and $Ag3d_{3/2}$, respectively. The difference (6.0 eV) of binding energy between $Ag3d_{3/2}$ and $Ag3d_{5/2}$ indicates that silver is metallic nature in the sample [21]. Peak positions of Ag3d shift remarkably to lower binding energies compared with those of bulk Ag ($Ag3d_{5/2}$, 368.2 eV and $Ag3d_{3/2}$, 374.2 eV), the similar results are also found in the previous work [9,13]. The binding energy shift of Ag is mainly attributed to electron transfer from

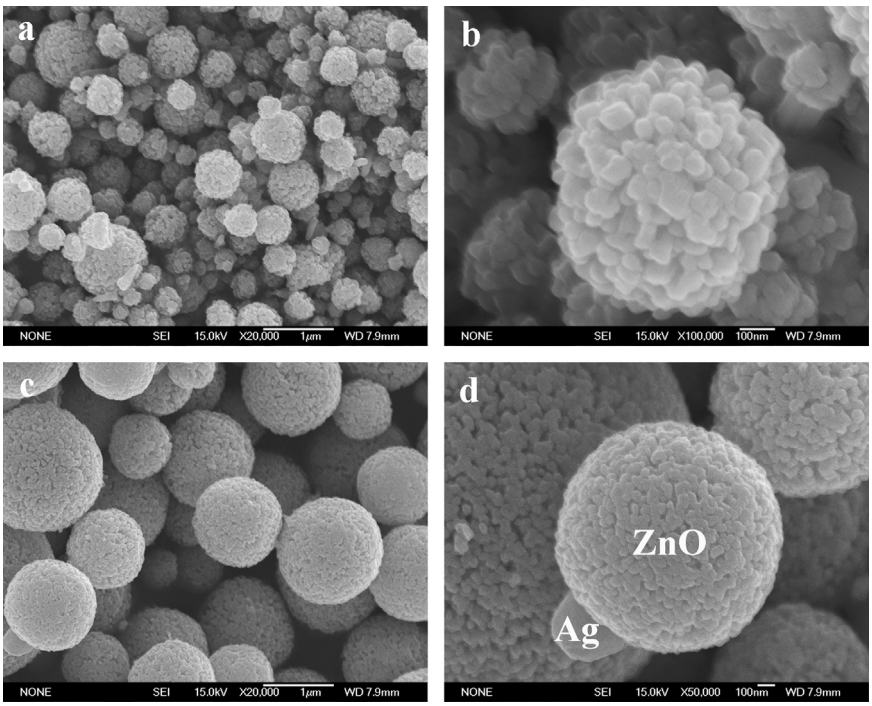

Fig. 2. SEM images of pure ZnO and Ag/ZnO composite with molar ratio of 1:150; (a), (c) low-magnification ZnO and Ag/ZnO; (b), (d) high-magnification ZnO and Ag/ZnO composite.

metallic Ag to ZnO crystals, resulting in the higher valence of Ag. Therefore, the shift to lower binding energies of Ag further verified the formation of Ag/ZnO heterostructure composites. The O1s XPS spectrum illustrated in Fig. 3d could be deconvoluted into two peaks. The peaks at 530.1 eV is ascribable to oxygen anions in the lattice of ZnO, while the peak centered at 531.5 eV is assigned to the chemisorbed oxygen of the surface hydroxyls [9].

3.4. UV–vis diffuse reflectance absorption spectra

Fig. 4 shows the comparison of UV–vis diffuse reflectance absorption spectra (DRS) of single ZnO and Ag/ZnO composites with different Ag contents. All of these samples presented the typical absorption with an intense transition in the UV region, which could be assigned to the intrinsic band-gap absorption of ZnO. The single ZnO showed no absorption above its fundamental absorption edge (around 400 nm). However, the absorption spectra of Ag/ZnO showed enhanced absorption in the visible-light region, which originated from the localized surface plasma resonance (LSPR) phenomenon of Ag nanoparticles loaded on the surface of ZnO [23].

3.5. Photocatalytic activity

Fig. 5 displays the photocatalytic activity of different catalysts (ZnO, Ag/ZnO and P25). For comparison, the blank test was also conducted under the same reaction conditions. It could be seen that the degradation percentage of RhB solution was very low in the absence of catalysts under UV light irradiation for 40 min. With the addition of catalysts, the degradation was greatly accelerated. The Ag/ZnO composites exhibited higher photocatalytic activity than that of the pure ZnO. This indicated the importance of Ag modification for improving photocatalytic performance of ZnO. Further observation showed that the photocatalytic activity gradually enhanced with increasing amount of Ag in the composites. Especially, when the molar ratio of Ag to ZnO was 1:150, the photocatalytic activity of Ag/ZnO composites significantly increased. However, further improving the amount of Ag in the composites, the photocataytic activity of Ag/ZnO composites

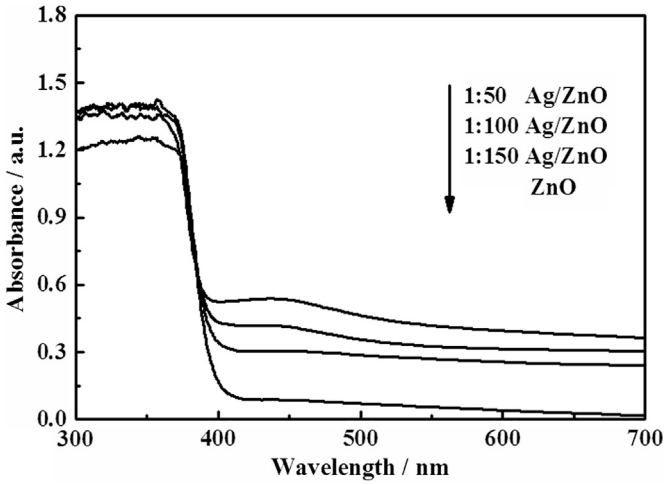

Fig. 4. UV–vis diffuse reflectance absorption spectra of pure ZnO and Ag/ZnO composites.

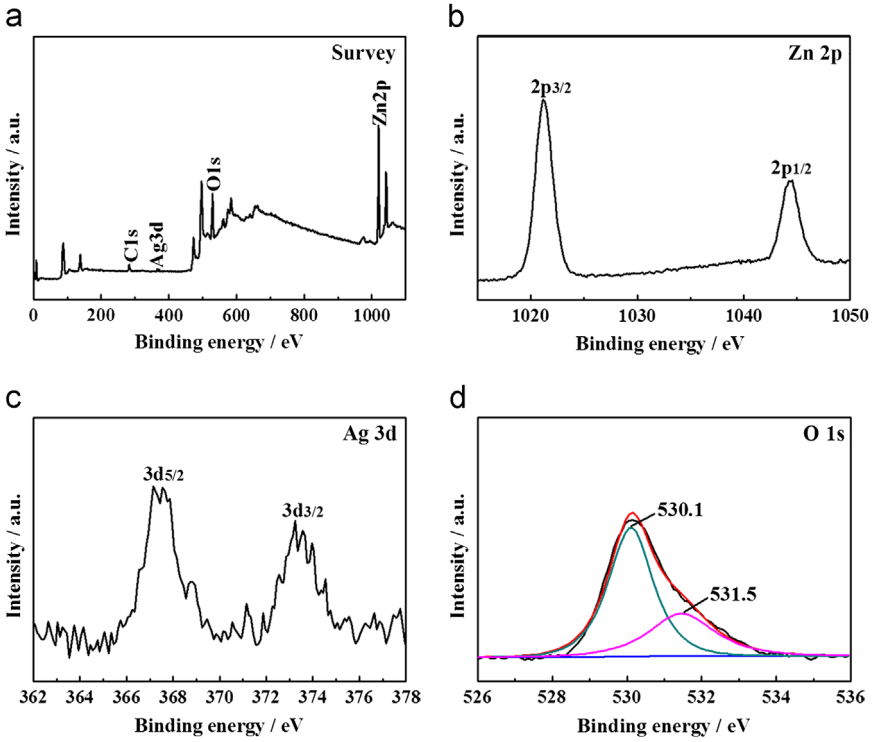

Fig. 3. XPS spectra of the 1:150 Ag/ZnO composite: XPS survey spectrum (a), high resolution Zn2p spectrum (b), high resolution Ag3d spectrum (c), and high resolution O1s spectrum (d).

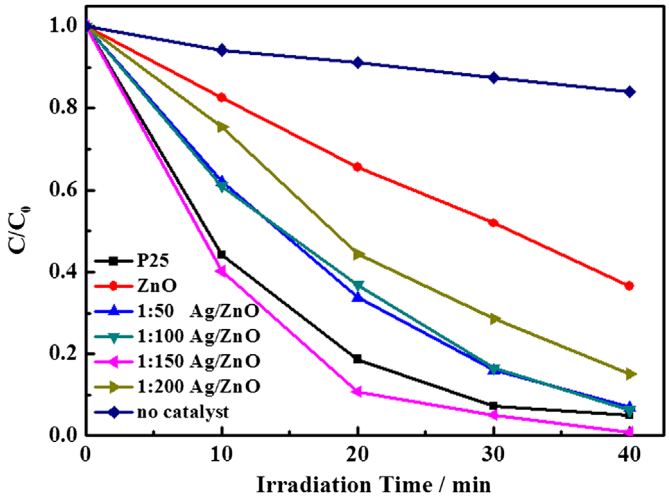

Fig. 5. Comparison of photocatalytic activity of the samples for degradation of RhB solution at ambient temperature; C and C_0 denote the reaction and initial concentration of RhB in the system, respectively.

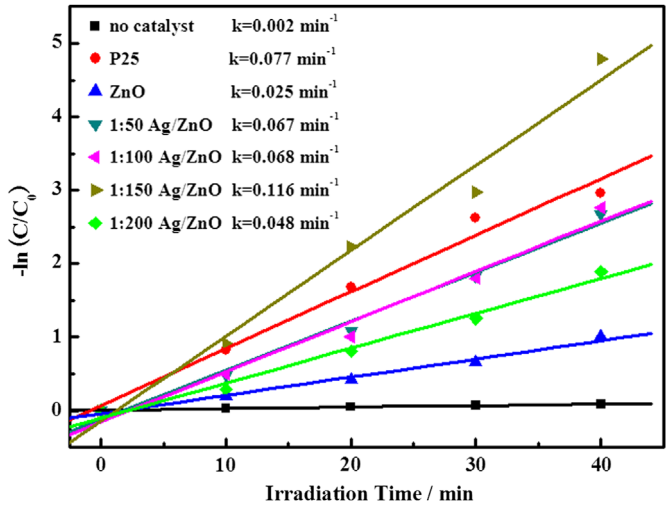

Fig. 6. Kinetic fit for the degradation of RhB by different samples.

obviously decreased. The photocatalytic activity of Degussa P25 was measured as a reference to compare with that of the synthesized catalysts. As shown, the degradation percentage of RhB by P25 was about 94.8% after irradiation for 40 min, which was lower than that of 1:150 Ag/ZnO composites. The results indicate that the 1:150 Ag/ZnO composites are superior to P25 for photocatalytic degradation of RhB dye.

Generally, the photocatalytic degradation of RhB can be considered as a pseudo-first order reaction with low concentration, and its kinetics can be expressed as follows:

$$-\ln(C/C_0) = kt \quad (1)$$

Where k is the degradation rate constant, C_0 and C are the initial concentration of RhB and the concentration of the pollution at a reaction time of t, respectively [13]. As shown in the Fig. 6, the rate constants (k) of different samples were 0.025, 0.048, 0.116, 0.068, 0.067, 0.077 and 0.002 min^{-1} for pure ZnO, 1:200 Ag/ZnO, 1:150 Ag/ZnO, 1:100 Ag/ZnO, 1:50 Ag/ZnO, P25 and without catalysts, respectively. The rate constant of Ag/ZnO composites firstly increased and then decreased with improving Ag amount in the composites. The loading of Ag with appropriate amount on ZnO surface can produce the Schottky barrier, which effectively capture and transfer the photogenerated electrons, and thus suppress the recombination of the photogenerated electron–hole pairs [24]. However, when the more Ag is loaded, the size increase of Ag particles will happen, which is disadvantageous to inhibit the recombination of the electron–hole pairs. On the other hand, the decrease in photocatalytic activity at higher Ag contents is considered to be related to the increased absorbing and scattering of photons by Ag in the photoreaction system.

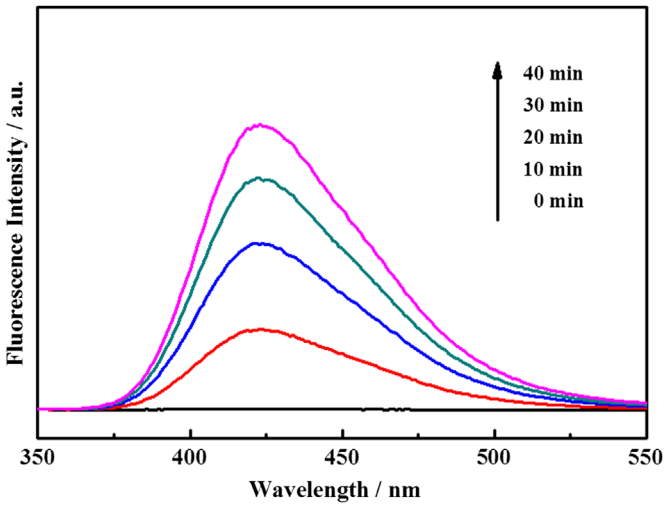

Fig. 7. PL spectral changes with UV light irradiation time on the Ag/ZnO composite in a 5×10^{-4} M basic solution of TA (excitation at 315 nm).

In order to understand the involvement of active species in the photocatalytic process, the formation of hydroxyl radicals (•OH) on the surface of catalysts was detected by the PL technique using terephthalic acid as a probe molecule. Fig. 7 shows the changes in the PL spectra for 5×10^{-4} M terephthalic acid solution in 2×10^{-3} M NaOH with irradiation time in the presence of 1:150 Ag/ZnO composite. As could be seen, a gradual increase in the PL intensity at about 425 nm was observed with increasing irradiation time. However, no PL intensity increase was observed in the absence of UV light or the photocatalyst. This suggested that the fluorescence was caused by chemical reactions of terephthalic acid with •OH formed at the catalyst/water interface *via* photocatalytic reactions [21].

As the photocatalytic process of the Ag/ZnO composite is complex, it is necessary to discuss the band structure of Ag/ZnO composite in detail. When the metallic Ag particles are attached to ZnO particles, as the Fermi energy level of Ag is higher than that of ZnO, it will lead to a migration of electrons from Ag to the conduction band (CB) of ZnO in order to achieve Fermi energy level equilibration (E_f). This process can be expressed as [13]

$$Ag \rightarrow Ag^+ + e^- \quad (2)$$

As is shown in Fig. 8, when the catalysts are illuminated by UV light with photon energy higher than the band gap of ZnO,

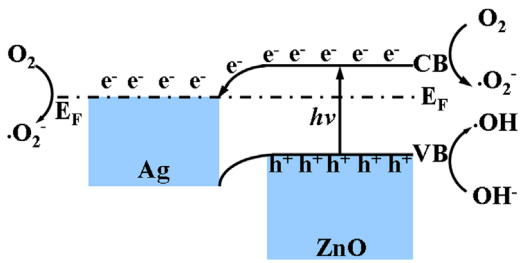

Fig. 8. Proposed schematic illustrations of the band structure related photocatalytic mechanism for the Ag/ZnO composite.

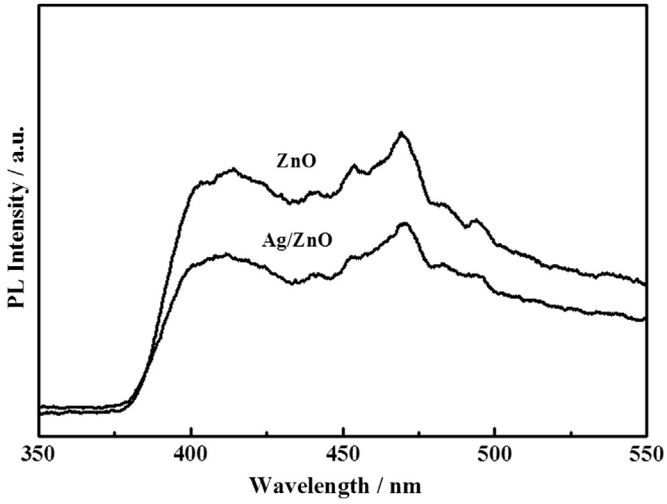

Fig. 9. PL spectra of pure ZnO and Ag/ZnO composite.

the photoexcited electrons and holes are formed in the CB and valence band (VB) of ZnO, respectively. Because the bottom energy level of the CB of ZnO is higher than the new equilibrium Fermi energy level (E_f) of Ag/ZnO, the electrons on the CB can transfer from ZnO to Ag nanoparticles. It has been proposed that the charge separation is the outcome of the Schottky barrier formed at the metal–semiconductor interface. Therefore, Ag nanoparticles, acting as electron sinks, reduce the recombination of photogenerated electrons and holes, and prolong the lifetime of the electron–hole pairs. Subsequently, the electrons can be captured by the adsorbed O_2, and the holes can be trapped by the surface hydroxyl, resulting in the formation of superoxide anion radical ($\bullet O_2^-$) and hydroxyl radical species ($\bullet$OH). Both radical groups ($\bullet O_2^-$ and $\bullet$OH) are highly reactive toward RhB degradation. The photocatalytic reaction process can be proposed as follows [13,15]:

$$ZnO + h\nu \rightarrow e^- + h^+ \quad (3)$$

$$e^- + O_2 \rightarrow \bullet O_2^- \quad (4)$$

$$Ag^+ + e^- \rightarrow Ag \quad (5)$$

$$h^+ + OH^- \rightarrow \bullet OH \quad (6)$$

In part, photocatalytic activity is a function of the lifetime and trapping of photogenerated electrons and holes in the semiconductor. The PL emission spectra are often employed to support the proposed mechanism [23]. Fig. 9 presents a comparison of the PL spectra of pure ZnO and Ag/ZnO composite with molar ratio of 1:150 in the wavelength range of 350–550 nm. The PL spectrum for ZnO was characterized by two main peaks around 410 and 470 nm, which attributed to the emission of band-gap transition and surface oxygen vacancies and defects, respectively. A fluorescence decrease was observed for Ag/ZnO composite indicating reduced charge recombination in comparison to ZnO alone. The results of PL verify that the Ag/ZnO composite could more effectively separate electron–hole pairs under light irradiation.

4. Conclusions

In summary, the Ag/ZnO heterostructure microspheres have been prepared *via* a simple one-pot TEA-assisted hydrothermal method. In this case, the TEA plays a dual role in the formation process of Ag/ZnO microspheres. The Ag/ZnO composites could promote the charge separation of photogenerated electrons and holes, and then improve the photocatalytic activity. Among the prepared composites, the Ag/ZnO with molar ratio of 1:150 exhibits the best photocatalytic activity for the degradation of RhB under UV illumination. The present method for constructing Ag/ZnO composites *via* a simple one-pot route is promising in the application for the preparation of other kinds of metal/semiconductor composites.

Acknowledgment

We acknowledge Prof. Tianyou Peng from Wuhan University for the materials property measurement. This work was supported by the Program for Introduction (Training) Talents of Wuhan Polytechnic University (2012RZ12).

References

[1] K. Rajeshwar, M.E. Osugi, W. Chanmanee, C.R. Chenthamarakshan, M. V.B. Zanoni, P. Kajitvichyanukul, R. Drishnan-Ayer, Heterogeneous photocatalytic treatment of organic dyes in air and aqueous media, Journal of Photochemistry and Photobiology C 9 (2009) 171–192.
[2] X.B. Chen, S.S. Mao, Titanium dioxide nanomaterials: synthesis, proerties, modifications, and applications, Chemical Reviews 107 (2007) 2891–2959.
[3] H.B. Lu, S.M. Wang, L. Zhao, J.C. Li, B.H. Dong, Z.X. Xu, Hierarchical ZnO microarchitectures assembled by ultrathin nanosheets: hydrothermal synthesis and enhanced photocatalytic activity, Journal of Materials Chemistry 21 (2011) 4228–4234.
[4] J.G. Yu, X.X. Yu, Hydrothermal synthesis and photocatalytic activity of zinc oxide hollow spheres, Environmental Science and Technology 42 (2008) 4902–4907.
[5] M.S. Wang, Y.P. Zhang, Y.J. Zhou, F.W. Yang, E.J. Kim, S.H. Hahn, S. G. Seong, Rapid room-temperature synthesis of nanosheet-assembled ZnO mesocrystals with excellent photocatalytic activity, CrystEngComm 15 (2013) 754–763.
[6] Z.M. Lam, J.C. Sin, A.Z. Abdullah, A.R. Mohamed, ZnO nanorods surface-decorated by WO_3 nanoparticles for photocatalytic degradation of endocrine disruptors under a compact fluorescent lamp, Ceramics International 39 (2013) 2343–2352.
[7] T.G. Xu, L.W. Zhang, H.Y. Cheng, Y.F. Zhu, Significantly enhanced photocatalytic performance of ZnO via graphene hybridization and the mechanism study, Applied Catalysis B: Environmental 101 (2011) 382–387.

[8] Y. Tak, H. Kim, D. Lee, K. Yong, Type-II CdS nanoparticle-ZnO nanowire heterostructure arrays fabricated by a solution process: enhanced photocatalytic activity, Chemical Communications 38 (2008) 4585–4587.
[9] W.W. Lu, S.Y. Gao, J.J. Wang, One-pot synthesis of Ag/ZnO self-assembled 3D hollow microspheres with enhanced photocatalytic performance, Journal of Physical Chemistry C 112 (2008) 16792–16800.
[10] C.G. Tian, W. Li, K. Pan, Q. Zhang, G.H. Tian, W. Zhou, H.G. Fu, One pot synthesis of Ag nanoparticle modified ZnO microspheres in ethylene glycol medium and their enhanced photocatalytic performance, Journal of Solid State Chemistry 183 (2010) 2720–2725.
[11] Y.L. Lai, M. Meng, Y.F. Yu, One-step synthesis, characterizations and mechanistic study of nanosheets-constructed fluffy ZnO and Ag/ZnO spheres used for Rhodamine B photodegradation, Applied Catalysis B: Environmental 100 (2010) 491–501.
[12] Y.H. Zheng, L.R. Zheng, Y.Y. Zhan, X.Y. Lin, Q. Zheng, K.M. Wei, Ag/ZnO heterostructure nanocrystals: synthesis, characterization, and photocatalysis, Inorganic Chemistry 46 (2007) 6980–6986.
[13] D.D. Lin, H. Wu, R. Zhang, W. Pan, Enhanced photocatalysis of electrospum Ag-ZnO heterostructured nanofibers, Chemistry of Materials 21 (2009) 3479–3484.
[14] S.Y. Gao, X.X. Jia, S.X. Yang, Z.D. Li, K. Jiang, Hierarchical Ag/ZnO micro/nanostructure: green synthesis and enhanced photocatalytic performance, Journal of Solid State Chemistry 184 (2011) 764–769.
[15] C.D. Gu, C. Cheng, H.Y. Huang, T.L. Wong, N. Wang, T.Y. Zhang, Growth and photocatalytic activity of dendrite-like ZnO@Ag heterostructure nanocrystals, Crystal Growth and Design 9 (2009) 3278–3285.
[16] T. Alammar, A.V. Mudring, Facile preparation of Ag/ZnO nanoparticles via photoreduction, Journal of Materials Science 44 (2009) 3218–3222.
[17] S. Xu, Z.H. Li, Q. Wang, L.J. Cao, T.M. He, G.T. Zou, A novel one-step method to synthesize nano/micron-sized ZnO sphere, Journal of Alloys and Compounds 465 (2008) 56–60.
[18] H. Jiang, J.Q. Hu, F. Gu, C.Z. Li, Large-scaled, uniform, monodispersed ZnO colloidal microspheres, Journal of Physical Chemistry C 112 (2008) 12138–12141.
[19] Y. Zeng, T. Zhang, W.Y. Fu, Q.J. Yu, G.R. Wang, Y.Y. Zhang, Y. M. Sui, L.J. Wang, C.L. Shao, Y.C. Liu, H.B. Yang, G.T. Zou, Fabrication and optical properties of large-scale nutlike ZnO microcrystals via a low-temperature hydrothermal route, Journal of Physical Chemistry C 113 (2009) 8016–8022.
[20] L.J. Cao, Z.H. Li, X.G. Hao, Y. Zhang, W.Q. Wang, Synthesis of Cu/Cu_2O core/multi-shelled microcrystal via shape and structure transformation of pre-grown crystals, Journal of Alloys and Compounds 475 (2009) 600–607.
[21] B. Cheng, Y. Le, J.G. Yu, Preparation and enhanced photocatalytic activity of Ag@TiO_2 core-shell nanocomposite nanowires, Journal of Hazardous Materials 177 (2010) 971–977.
[22] J.G. Yu, B. Wang, Effect of calcinations temperature on morphology and photoelectrochemical properties of anodized titanium dioxide nanotube arrays, Applied Catalysis B: Environmental 94 (2010) 295–302.
[23] J.G. Yu, L.F. Qi, M. Jaroniec, Hydrogen production by photocatalytic water splitting over Pt/TiO_2 nanosheets with exposed (001) facets, Journal of Physical Chemistry C 114 (2010) 13118–13125.
[24] J.G. Yu, J.F. Xiong, B. Cheng, S.W. Liu, Fabrication and characterization of Ag–TiO_2 multiphase nanocomposite thin films with enhanced photocatalytic activity, Applied Catalysis B: Environmental 60 (2005) 211–221.